*remote sensing*

MDPI

*Article*

# Soil Moisture Mapping from Satellites: An Intercomparison of SMAP, SMOS, FY3B, AMSR2, and ESA CCI over Two Dense Network Regions at Different Spatial Scales

**Chenyang Cui [1,2], Jia Xu [1], Jiangyuan Zeng [2,*], Kun-Shan Chen [2], Xiaojing Bai [3], Hui Lu [4,5], Quan Chen [6] and Tianjie Zhao [2]**

1 School of Earth Sciences and Engineering, Hohai University, Nanjing 210098, China; 151311030007@hhu.edu.cn (C.C.); hhuxj@hhu.edu.cn (J.X.)
2 State Key Laboratory of Remote Sensing Science, Jointly Supported by Institute of Remote Sensing and Digital Earth, Chinese Academy of Sciences and Beijing Normal University, Beijing 100101, China; chenks@radi.ac.cn (K.-S.C.); zhaotj@radi.ac.cn (T.Z.)
3 School of Hydrology and Water Resources, Nanjing University of Information Science and Technology, Nanjing 210044, China; baixiaojing1219@126.com
4 Ministry of Education Key Laboratory for Earth System Modeling, Department of Earth System Science, Tsinghua University, Beijing 100084, China; luhui@tsinghua.edu.cn
5 The Joint Center for Global Change Studies, Beijing 100875, China
6 Airborne Remote Sensing Center, Institute of Remote Sensing and Digital Earth, Chinese Academy of Sciences, Beijing 100094, China; chenquan@radi.ac.cn
* Correspondence: zengjy@radi.ac.cn

Received: 2 November 2017; Accepted: 23 December 2017; Published: 25 December 2017

**Abstract:** A good knowledge of the quality of the satellite soil moisture products is of great importance for their application and improvement. This paper examines the performance of eight satellite-based soil moisture products, including the Soil Moisture Active Passive (SMAP) passive Level 3 (L3), the Soil Moisture and Ocean Salinity (SMOS) Centre Aval de Traitement des Données SMOS (CATDS) L3, the Japan Aerospace Exploration Agency (JAXA) Advanced Microwave Scanning Radiometer 2 (AMSR2) L3, the Land Parameter Retrieval Model (LPRM) AMSR2 L3, the European Space Agency (ESA) Climate Change Initiative (CCI) L3, the Chinese Fengyun-3B (FY3B) L2 soil moisture products at a coarse resolution of ~0.25°, and the newly released SMAP enhanced passive L3 and JAXA AMSR2 L3 soil moisture products at a medium resolution of ~0.1°. The ground soil moisture used for validation were collected from two well-calibrated and dense networks, including the Little Washita Watershed (LWW) network in the United States and the REMEDHUS network in Spain, each with different land cover. The results show that the SMAP passive soil moisture product outperformed the other products in the LWW network region, with an unbiased root mean square (ubRMSE) of 0.027 $m^3$ $m^{-3}$, whereas the FY3B soil moisture performed the best in the REMEDHUS network region, with an ubRMSE of 0.025 $m^3$ $m^{-3}$. The JAXA product performed much better at 0.25° than at 0.1°, but at both resolutions it underestimated soil moisture most of the time (bias < −0.05 $m^3$ $m^{-3}$). The SMAP-enhanced passive soil moisture product captured the temporal variation of ground measurements well, with a correlation coefficient larger than 0.8, and was generally superior to the JAXA product. The LPRM showed much larger amplitude and temporal variation than the ground soil moisture, with a wet bias larger than 0.09 $m^3$ $m^{-3}$. The underestimation of surface temperature may have contributed to the general dry bias found in the SMAP (−0.018 $m^3$ $m^{-3}$ for LWW and 0.016 $m^3$ $m^{-3}$ for REMEDHUS) and SMOS (−0.004 $m^3$ $m^{-3}$ for LWW and −0.012 $m^3$ $m^{-3}$ for REMEDHUS) soil moisture products. The ESA CCI product showed satisfactory performance with acceptable error metrics (ubRMSE < 0.045 $m^3$ $m^{-3}$), revealing the effectiveness of merging active and passive soil moisture products. The good performance of SMAP and FY3B demonstrates the

potential in integrating them into the existing long-term ESA CCI product, in order to form a more reliable and useful product.

**Keywords:** soil moisture; SMAP; FY3B; SMOS; AMSR2; ESA CCI; comparison

## 1. Introduction

Over the past few decades, a series of active and passive microwave satellites or sensors, e.g., the Advanced Scatterometer (ASCAT) [1], the Advanced Microwave Scanning Radiometer-Earth Observing System (AMSR-E) [2], the Advanced Microwave Scanning Radiometer 2 (AMSR2) [3], the Soil Moisture and Ocean Salinity (SMOS) mission [4], and the Soil Moisture Active Passive (SMAP) mission [5] have been successfully launched, and are able to monitor soil moisture both spatially and temporally. Various satellite soil moisture products have been freely released to the public since the early 2000s [2,6]. The L-band (1–2 GHz) has been recognized as the optimal band for soil moisture retrieval, since the influence of atmosphere can be minimized and less energy is absorbed or reflected by vegetation at this band [7]. The SMAP mission [5] and the SMOS mission [4] are now the only two soil moisture-dedicated satellites in orbit that are equipped with L-band microwave instruments. In addition to L-band satellites, there has already been a long heritage of soil moisture products retrieved from higher frequencies, such as C-band and X-band, though these are not optimal for soil moisture estimation, since they are more vulnerable to the effects of vegetation compared to the L-band. It has been more than ten years since the first standard soil moisture product was delivered from the Advanced Microwave Scanning Radiometer–Earth Observing System (AMSR-E) [2]. Over the last few decades, soil moisture retrieval algorithms have been continuously developed and improved for both active and passive sensors and satellites, including the Advanced Scatterometer (ASCAT), the AMSR-E and its successor AMSR2, the WindSat, the Aquarius, the SMAP and SMOS satellites, and the Chinese Fengyun-3B (FY3B) satellite [2,6,8–12]. The FY3B is China's second-generation polar-orbiting meteorological satellite, and the first in the FY3 satellite series that carries a Microwave Radiation Imager (MWRI) in order to observe the Earth's surface with five different frequencies, ranging from 10.65 GHz to 89 GHz [13]. Additionally, in response to the requirement for a long-term and globally remotely sensed soil moisture record, the European Space Agency (ESA) introduced soil moisture to their Climate Change Initiative (CCI) program, and developed the first multi-satellite soil moisture dataset, i.e., the ESA CCI soil moisture product [14,15].

As soil moisture retrieval algorithms are gradually refined, satellite soil moisture products have been updated continuously. Therefore, the examination of the error characteristics and limitations of various new soil moisture products is becoming increasingly important, as it not only helps users make optimal use of these products, but also identifies possible deficiencies in the products and further improves the algorithms [16]. Extensive validation activities for various satellite soil moisture products have been conducted in recent years (e.g., [16–28]). Jackson et al. [20,21] validated four AMSR-E soil moisture products, i.e., National Aeronautics and Space Administration (NASA), Land Parameter Retrieval Model (LPRM), Single Channel Algorithm (SCA), and Japan Aerospace Exploration Agency (JAXA) [20], as well as the ESA SMOS soil moisture product (algorithm v.400) [21] using in-situ measurements from four watershed networks in the United States where they found that SCA performs the best out of the four AMSR-E products, and is generally comparable to that of SMOS, with an overall root-mean-square error (RMSE) of 0.043 $m^3$ $m^{-3}$. Zeng et al. [16] conducted a comprehensive evaluation of state-of-the art soil moisture products (i.e., ESA CCI, ASCAT, LPRM, JAXA, NASA, AMSR2, SMOS, and ERA-Interim) over the Tibetan Plateau, and found that the ESA CCI and ERA-Interim products generally outperformed the other products, with the highest correlation coefficient value of 0.77 and the lowest RMSE of 0.079 $m^3$ $m^{-3}$, respectively, on the highest plateau in the world. Al-Yaari et al. [22] compared SMOS and AMSR-E soil moisture products with respect

to land data assimilation system estimates on a global scale, and found that SMOS products were generally superior to AMSR-E, especially in highly vegetated areas. With the recently launched SMAP mission, more focus has been placed on the validation of the new SMAP product (e.g., [23–25]), and the results generally showed a very promising performance of SMAP, though continued bias (e.g., the bias ranged from $-0.088$ $m^3$ $m^{-3}$ to 0.072 $m^3$ $m^{-3}$ in [24] calculated from 13 core validation sites) is observed in the product. Very limited studies examine the quality of the Chinese FY3B soil moisture product. Parinussa et al. [15] first compared the FY3B soil moisture derived from LPRM and the official FY3B product, and found the two products could capture the temporal variation of soil moisture well at nighttime, with a high correlation coefficient larger than 0.6. Since a combination of multiple and reliable soil moisture products can significantly increase the temporal sampling of soil moisture observations, which is very beneficial to many hydro-meteorological applications, it is imperative that the accuracy of various satellite soil moisture products is evaluated, in order to gain knowledge of their error characteristics and limitations. Furthermore, most work has only focused on the assessment of soil moisture products at a relatively coarse spatial resolution of approximately 0.25°. More recently, the SMAP team released an enhanced passive soil moisture product, which has a grid resolution of 9 km, the same as the SMAP active-passive product. In our study, the potential benefit of this new product is examined, along with the comparison of JAXA AMSR2 soil moisture product at a similar resolution of 0.1°.

In this paper, we conduct a detailed examination of the quality of eight satellite soil moisture products at two typical spatial resolutions, including a comparison of SMAP passive, SMOS, JAXA AMSR2, LPRM AMSR2, ESA CCI, and the Chinese FY3B soil moisture products at a coarse resolution of approximately 0.25°, and the newly released SMAP enhanced passive and JAXA AMSR2 soil moisture products at a medium resolution of approximately 0.1°. To achieve these purposes, in-situ measurements from two representative dense networks, i.e., the Little Washita Watershed (LWW) and REMEDHUS networks are used to compare and validate the eight soil moisture products. Possible error sources in the satellite soil moisture products are also investigated and discussed in detail in this study. The paper is structured as follows: Section 2 briefly introduces the study area, in-situ observations, and satellite soil moisture products. Section 3 describes the evaluation method used in the paper. Section 4 presents the results of the comparison between satellite products and their in-situ measurements. Section 5 discusses the possible error sources in the soil moisture products, followed by the conclusions of this paper drawn in Section 6.

## 2. Data

### *2.1. Study Area and In-Situ Soil Moisture Data*

In this paper, in-situ soil moisture data were collected from two well-calibrated and dense networks, being the LWW network [29] in the United States and the REMEDHUS network [30] in Spain. The locations of the two networks and their corresponding sites are shown in Figure 1. The reasons for selecting the two network regions as our study areas consist of two aspects. First, high-quality and dense in-situ measurements can be measured from both networks, which can reduce the scale-related issue between the ground-based point and satellite pixel. It is known that soil moisture has high spatial variability, thus measurements from a single station cannot generally represent the retrievals of a satellite pixel. Fortunately, dense in-situ measurements can be measured in the two network regions, and the averaged spatial measurements from multiple stations can therefore reduce the inherent spatial issue as much as possible [16,20,21]. Second, the two network regions have different land covers (i.e., grasslands in LWW and croplands in REMEDHUS, see the Moderate Resolution Imaging Spectroradiometer (MODIS) International Geosphere Biosphere Program (IGBP) land cover in Figure 1), which can provide a more robust evaluation of the satellite soil moisture products. The details of the two networks are described below.

(1) *LWW Network*: The LWW network was built between Chickasha and Lawton, and is situated within the Great Plains region of the United States, with an area of 611 $km^2$. Currently, it consists of 20

stations, which measure soil moisture at 5, 25, and 45 cm below the surface and soil temperature at 5, 10, 15, 25, 30, and 45 cm in 5-min intervals. The climate of this region is sub-humid, with a stable annual precipitation of 760 mm. The LWW area is moderately rolling, with elevations ranging from 300 m to 500 m, and is mainly covered by grassland, with a wide range of soil textures from fine sand to silty loam. The LWW network has been widely used for monitoring hydrological and meteorological measurements since 1961. It has been extensively used for assessing satellite soil moisture products, due to the large dynamic range of soil moisture and flat terrain in this region [20,21,23,31].

(2) *REMEDHUS Network*: The REMEDHUS network is a dense network in Spain, which is located in the central semiarid sector of the Duero Basin, with an area of 1300 km$^2$. It is composed of 20 stations that measure soil moisture and surface temperature at 5 cm in 60-min intervals. These data are collected and updated continuously via the International Soil Moisture Network (ISMN) [32]. Croplands and shrublands dominate the land cover of this region. The land usage of the REMEDHUS network region is covered by cereals (78%), forest and pasture (13%), irrigated crops (5%), and vineyards (3%) [30]. The elevation of this region ranges from 700 to 900 m above sea level, with a continental semiarid Mediterranean climate, which brings dry and warm summers and cool and wet winters to this region [33,34]. The mean annual rainfall and average temperature of this region are 385 mm and 12 °C, respectively. The REMEDHUS network has a long history of hydrological-related applications, including the validation of satellite soil moisture products [30,35], the evaluation of soil moisture downscaling algorithm [36,37], and parameterization of water balance models [38].

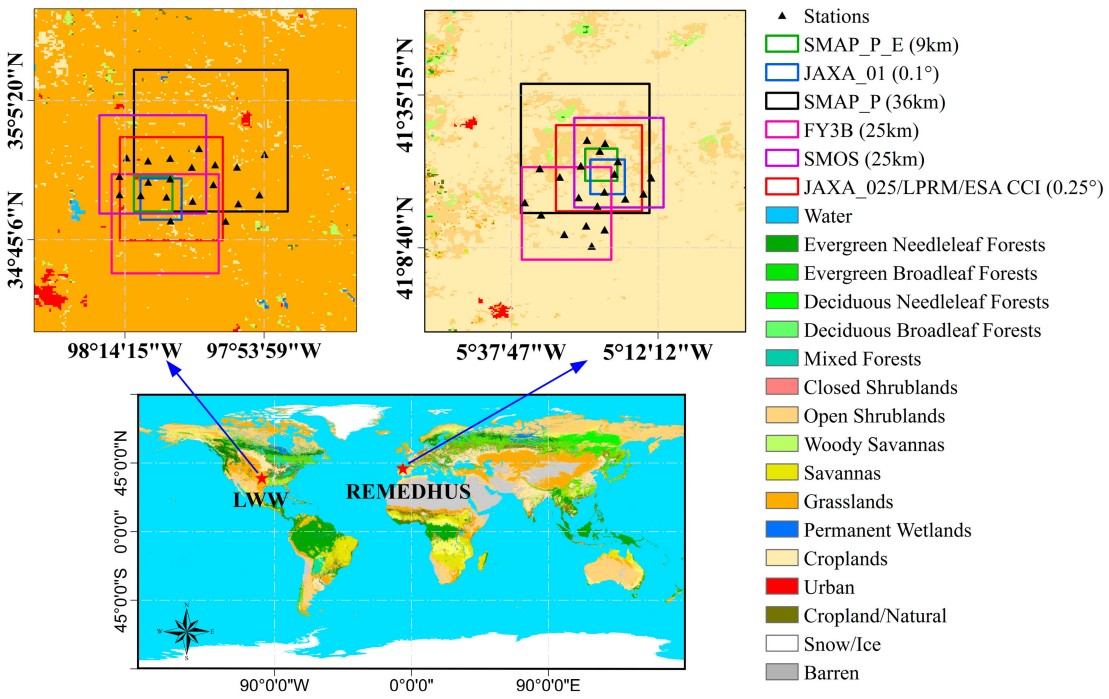


**Figure 1.** Location of the Little Washita Watershed (LWW) and REMEDHUS networks, the distribution of the corresponding stations, and the satellite pixel locations in each network. The legend of the color map denotes the Moderate Resolution Imaging Spectroradiometer (MODIS) International Geosphere Biosphere Program (IGBP) global land cover classes.

In our study, the precipitation data from the LWW network region we used were the in-situ measurements. Since the rainfall observations of the REMEDHUS network region are not available, we use the ERA-Interim daily rainfall product.

### *2.2. Satellite Soil Moisture Products*

#### 2.2.1. SMAP Passive and Enhanced Passive Soil Moisture Products

The SMAP satellite, which is the newest soil moisture-dedicated satellite in orbit, was launched by NASA on 31 January 2015. The instruments carried by SMAP consist of an L-band radar and an L-band radiometer. The local equatorial overpass time of the SMAP satellite is 6:00 P.M. (ascending) and 6:00 A.M. (descending). SMAP provides a total of four remotely-sensed soil moisture products, which are the passive, the active, the active-passive, and the enhanced passive soil moisture product, which is a newly released product with the same grid resolution (9 km) as the active-passive product. Since the SMAP radar ceased operations in July 2015, resulting in only a short period of time with the active and active-passive soil moisture products, we choose the SMAP passive and enhanced passive soil moisture products, which have run from 31 March 2015 to the present, for evaluation. The two SMAP products can be downloaded freely from the National Snow and Ice Data Center (NSIDC) (https://nsidc.org/data/smap/smap-data.html).

The daily SMAP passive level-3 product (version 4) with a spatial resolution of 36 km, generated on EASE-Grid 2.0, is used in this paper. The V-pol single channel algorithm (SCA-V) is the current baseline retrieval algorithm of the SMAP passive soil moisture product [23,24]. Aside from SCA-V, the SMAP algorithm team also considers four other algorithms, including the H-pol single channel algorithm (SCA-H), the land parameter retrieval model (LPRM), the dual channel algorithm (DCA), and the extended DCA. In SCA-V, soil moisture can be retrieved from SMAP brightness temperature by the following five steps. First, the brightness temperature is normalized to apparent emissivity, by using surface temperature auxiliary data derived from the Goddard Earth Observing System (GEOS)-5 model to remove the effects of soil and vegetation physical temperature. Second, the vegetation effects are corrected using MODIS normalized difference vegetation index (NDVI) auxiliary data. Third, the soil surface roughness effects are corrected by applying a semi-empirical roughness model, known as the Hp model [39]. Fourth, the Fresnel equations are adopted to convert emissivity to soil permittivity. Finally, soil permittivity is converted to soil moisture, by using the Mironov dielectric model [40]. For more details about the SCA-V algorithm, readers are referred to [11,41].

The SMAP enhanced passive soil moisture product was recently released to the public. The daily SMAP enhanced passive level-3 product (version 1), with a grid resolution of 9 km generated on EASE-Grid 2.0, is used in our study. The SMAP enhanced soil moisture is retrieved from the interpolated SMAP brightness temperature observations at 9 km. This is because the SMAP radiometer sampling provides overlapping observations along the scan and along the track, which makes reconstructing the observed scene with improved resolution possible [42]. The original SMAP brightness temperatures at a coarse resolution of 36 km are converted to a medium resolution of 9 km, by applying the Backus-Gilbert optimal interpolation technique [43], since it is able to extract maximum information from SMAP antenna temperatures. Then, the SMAP enhanced soil moisture is obtained from the interpolated brightness temperature, using the SCA-V algorithm. More details about the SMAP enhanced passive soil moisture product can be found in [44].

#### 2.2.2. FY3B Soil Moisture Product

The FY3B satellite was launched by the China National Space Administration (CNSA) on 4 November 2010, and is equipped with a passive microwave radiometer which observes the Earth's surface on ten channels. A passive microwave radiometer called MWRI is on board the FY3B, which provides observations with frequencies ranging from 10.7 GHz to 89.0 GHz, and scans the Earth's surface in an ascending (1:40 P.M.) and descending (1:40 A.M.) mode. The satellite orbits at an altitude of 836 km, and scans the Earth with an incidence angle of 55.4°, leading to 1400 km wide swaths. The daily FY3B level-3 product, with a grid resolution of 25 km generated on original EASE-Grid (1.0), is used in this study. The FY3B soil moisture is released to the public by the

Chinese National Satellite Meteorological Center (CNSMC) and can be obtained freely after registration (http://satellite.nsmc.org.cn/portalsite/default.aspx).

In the current FY3B official algorithm, the X-band (10.7 GHz) brightness temperature at both V and H polarizations are used to obtain the soil moisture. The effects of surface temperature are firstly corrected from the Ka-band (36.5 GHz) vertical polarized brightness temperature [45]. The vegetation optical depth is then estimated based on an empirical relationship between the NDVI and the vegetation water content (VWC) [46], a similar step to one used in the SMAP SCA-V algorithm. A significant difference between the FY3B retrieval algorithm and other algorithms is that the FY3B utilizes a new surface emission model (i.e., the Qp model) [47] which is parameterized using the Advanced Integral Equation Model (AIEM) [48], a well-established theoretical model to correct the effects of surface roughness. Shi et al. [49] found that the impacts of surface roughness on microwave emission at large look angles were different in both magnitude and direction at the H and V polarizations. That is, the H-polarized microwave emissivity will increase, while the V-polarized emissivity will decrease, as surface roughness increases. Thus, the effects of surface roughness can be minimized by combining the emission signals from the two polarizations. Apart from brightness temperature, the ancillary data, including soil texture data, and global land surface classification data are involved in the soil moisture retrieval algorithm. More details about FY3B soil moisture algorithm can be found in [49].

#### 2.2.3. SMOS Soil Moisture Product

The SMOS satellite, which carries an interferometric L-band (1.4 GHz) radiometer, was launched by the ESA on 2 November 2009. SMOS monitors the global near-surface soil moisture every three days, with the ascending orbit at 6:00 A.M. (local solar time) and the descending orbit at 6:00 P.M. (local solar time). In the study, the daily SMOS level-3 soil moisture product with a grid resolution of 25 km, generated on EASE-Grid 2.0 from the Centre Aval de Traitement des Données SMOS (CATDS) and the Centre National d'Etudes Spatiales (CNES), was used.

In the SMOS retrieval algorithm, multi-angular brightness temperature observations are used to retrieve soil moisture and vegetation optical depth simultaneously, by minimizing the difference between the observed and estimated brightness temperature. The L-band Microwave Emission of Biosphere (L-MEB) model [50], which is based on a zero-order radiative transfer equation, is selected as the forward model. The soil temperature inputs are derived from the European Centre for Medium-Range Weather Forecasts (ECMWF) model. The SMOS measurements used in this study were filtered by two conditions: (i) the Data Quality IndeX (DQX) >0.1, and (ii) the probability of radio frequency interference (RFI_Prob) >0.2 [51]. More details about the SMOS retrieval algorithm can be found in [9].

#### 2.2.4. AMSR2 Soil Moisture Products

AMSR2 was carried on the Global Change Observation Mission-1st Water (GCOM-W1) satellite. It was launched by the Japan Aerospace Exploration Agency (JAXA) on 18 May 2012, and started to acquire scientific observations on 3 July 2012. It scans the Earth's surface in an ascending (1:30 P.M. local solar time) and descending (1:30 A.M. local solar time) mode. AMSR-2 is a successor to the AMSR-E, which operated from May 2002 to October 2011, and provided the first standard soil moisture product [2,16]. AMSR2 provides passive microwave measurements on fourteen channels, with frequencies ranging from 6.9 GHz to 89.0 GHz at H and V polarizations. Two soil moisture products derived from AMSR2, i.e., the JAXA and LPRM soil moisture products, are released to the public, and therefore used in the study.

The JAXA AMSR2 provides soil moisture product at two spatial resolutions, i.e., 0.1° and 0.25°. In the study, the two JAXA Level 3 soil moisture standard products from GCOM-W1 Data Providing Service (https://gcom-w1.jaxa.jp/auth.html) were used. The JAXA AMSR2 retrieval algorithm estimates surface soil moisture by using a lookup table method and multi-channel brightness temperatures. In the JAXA algorithm, a brightness temperature database, which covers a wide range

of vegetation and soil conditions for multiple frequencies and polarizations, is generated by using a forward radiative transfer scheme. These datasets are used to create lookup tables, by assuming a constant surface temperature of 293 K. Soil moisture is estimated by using the microwave polarization ratio (PI) at 10.65 GHz and the index of soil wetness (ISW) at 36.5 GHz and 10.65 GHz horizontal channels. For more details about the JAXA algorithm, readers are referred to [52].

The LPRM AMSR2 is delivered at a spatial resolution of 0.25° and is retrieved by the LPRM algorithm [12]. Similar to FY3B algorithm, LPRM uses Ka-band V-pol brightness temperature to estimate land surface temperature [53]. Soil moisture and vegetation optical depth are retrieved simultaneously through a nonlinear iterative procedure by applying the microwave PI. In LPRM, both C-band and X-band observations are used to obtain soil moisture retrievals. Li et al. [54] and Njoku et al. [55] found that the C-band microwave observations were heavily affected by the radio-frequency interference (RFI) over a large part of the United States and some parts of Europe. Thus, to minimize the uncertainties originated from RFI, we use the LPRM X-band soil moisture product. The LPRM data can be obtained freely from the Goddard Earth Sciences Data and Information Services Center (GES DISC) (https://gcmd.gsfc.nasa.gov/). For more details about the LPRM algorithm, readers are referred to [12].

#### 2.2.5. ESA CCI Soil Moisture Product

The ESA CCI soil moisture product (previously called the ECV soil moisture product), which is combined from active and passive microwave soil moisture retrievals, is a global, daily, long-term soil moisture record developed by the ESA, with a spatial resolution of 0.25°. In the study, the latest-released ESA CCI soil moisture v03.3 product, with a span of over 38 years, from November 1978 to December 2016, is used. The ESA CCI soil moisture v03.3 consists of three datasets, including the active, passive, and combined active and passive soil moisture products. The active soil moisture product is produced by microwave scatterometers, i.e., scatterometers (SCAT) and ASCAT, using the change detection method (TU Wien WARP v5.5). The passive soil moisture product is produced by microwave radiometers including Scanning Multichannel Microwave Radiometer (SMMR), Special Sensor Microwave Imager (SSM/I), Tropical Rainfall Measuring Mission Microwave Imager (TMI), AMSR-E, WindSat, AMSR-2, and SMOS by utilizing the LPRM. The combined soil moisture product is blended based on the active and passive soil moisture products, using signal-to-noise ratio analysis to estimate the integration weights. Only the combined (active-passive) ESA CCI is used in this paper. More details of the ESA CCI soil moisture product can be found in [14,56].

## 3. Methods

In this study, in-situ measurements from dense stations in both the LWW and REMEDHUS networks were used to examine the performance of eight satellite soil moisture products, including the SMAP passive soil moisture product at 36 km, the SMAP enhanced passive soil moisture product at 9 km, the SMOS soil moisture product at 25 km, the JAXA AMSR2 soil moisture product at 0.25° and 0.1°, the LPRM AMSR2 soil moisture product at 0.25°, the ESA CCI soil moisture product at 0.25°, and the FY3B soil moisture product at 25 km. The accuracy of satellite soil moisture products at two spatial scales including a coarse spatial resolution (approximately 25 km) and a medium spatial resolution (approximately 10 km) is compared in this study. For a consistent and fair comparison, in our study we use the nearest interpolation method to resample the SMAP passive, the SMOS, and the FY3B soil moisture products to a spatial resolution of 0.25°, the same as that of JAXA or LPRM AMSR2 and ESA CCI, as well as to resample the SMAP enhanced passive soil moisture to a spatial resolution of 0.1°, the same as that of JAXA AMSR2. The same method has been applied in many comparison studies of soil moisture products [16,22,57,58]. The blue grid at a 0.1° resolution and the red grid at a 0.25° resolution, shown in Figure 1, were selected as the validation grids in this study, since they contain the most stations in the two network regions. The blue grid and the red grid involve fours stations and thirteen stations in the LWW network, respectively, and involve three stations and eleven stations in

the REMEDHUS network, respectively. To reduce the spatial resolution inconformity of the satellite soil moisture products and ground observations, the station averaged in-situ measurements within the validation grid were used to evaluate the satellite soil moisture products within the corresponding grids [16,20,21]. Since the ESA CCI soil moisture was available through 31 December 2016, and the SMAP passive and enhanced passive soil moisture started on 31 March 2015, in order to make a fair comparison, all satellite soil moisture products were compared during the period from 1 April 2015 to 31 December 2016, which covers more than one and a half years.

The error metrics we used in the study include the root mean square error (RMSE), the correlation coefficient (R), the bias and the unbiased RMSE (ubRMSE) [59], which are defined as follows:

$$RMSE = \sqrt{E\langle(\theta_{satellite}(t) - \theta_{in-situ}(t))^2\rangle} \quad (1)$$

$$ubRMSE = \sqrt{E\langle((\theta_{satellite}(t) - E\langle\theta_{sateliite}(t)\rangle) - (\theta_{in-situ}(t) - E\langle\theta_{in-situ}(t)\rangle))^2} \quad (2)$$

$$Bias = E\langle\theta_{satellite}(t)\rangle - E\langle\theta_{in-situ}(t)\rangle \quad (3)$$

$$R = \frac{E\langle(\theta_{satellite}(t) - E\langle\theta_{satellite}(t)\rangle) \cdot (\theta_{in-situ}(t) - E\langle\theta_{in-situ}(t)\rangle)\rangle}{\sigma_{satellite} \cdot \sigma_{in-situ}} \quad (4)$$

where $E\langle\cdot\rangle$ is the representation of the linear averaging operator, $t$ is the time of observations, $\theta_{satellite}(t)$ represents the satellite soil moisture products at time $t$, $\theta_{in-situ}(t)$ represents the true observation based on the averaged ground measurements at time $t$. In addition, $\sigma_{satellite}$ and $\sigma_{in-situ}$ represent the standard deviation of eight satellite soil moisture measurements and ground observations, respectively. Furthermore, in our study, the $p$-value is also adopted to determine the significance level of the correlation coefficient.

The Taylor diagram [60] has been used to provide a brief statistical summary of how closely the datasets match observations in this paper, since the diagram can demonstrate the performance of various products in a single diagram in terms of the correlation coefficient, centered RMSE (i.e., ubRMSE), and standard deviation. During nighttime or morning time (e.g., from 0:00 A.M. to 6:00 A.M.), the thermal equilibrium builds up among the vegetation, air, and topsoil, which makes the basic assumption that vegetation temperature and topsoil temperature are equal in the soil moisture retrieval algorithms more reliable. Therefore, all satellite soil moisture products—except the ESA CCI product, which is provided on a daily basis—are evaluated at their nighttime or morning time overpass (i.e., 6:00 A.M. for SMAP and SMOS, 1:30 or 1:40 A.M. for FY3B and AMSR2, daily for ESA CCI). Figure 2 shows the temporal behavior of the station-averaged soil moisture at different times (daily, 1:30 A.M. and 6:00 A.M.) for the two network regions. It can be seen that the difference between the ground station-averaged soil moisture at different times is very small. That is to say, the time series, station-averaged soil moisture measurements at 1:30 A.M. and at 6:00 A.M. are nearly equal, which are also nearly equal to the daily station-averaged soil moisture measurements. Therefore, we use the daily, station-averaged in-situ measurements to examine the performance of the satellite soil moisture products in our study [16,19].

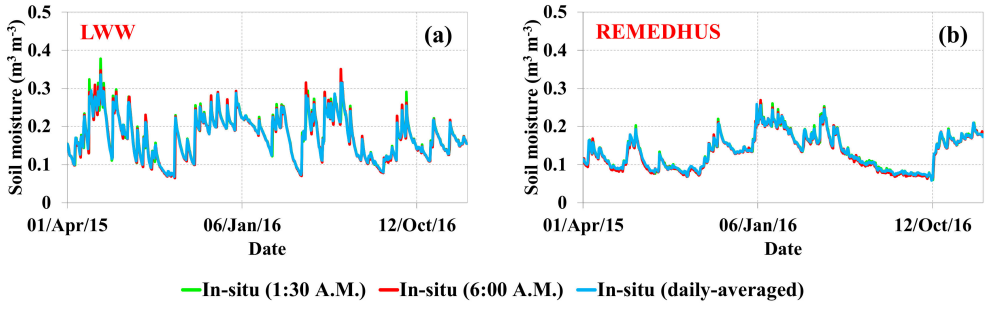


**Figure 2.** Temporal evolution of the station-averaged soil moisture at different times (daily, 1:30 A.M. and 6:00 A.M.) for (**a**) LWW, and (**b**) REMEDHUS.

## 4. Results

In this section, we analyze and discuss the performance of the eight satellite soil moisture products over the two dense network regions. First, we compare the temporal variation of ground observations with satellite products at two different spatial scales (i.e., 0.25° and 0.1°), as shown in Figures 3 and 4, respectively. The error metrics (i.e., RMSE, Bias, ubRMSE, and *R*) of satellite soil moisture products at 0.25° and 0.1° are summarized in Tables 1 and 2 respectively. The Taylor diagrams, which further reveal the statistics of comparison between the soil moisture products and ground measurements, are displayed in Figures 5 and 6.

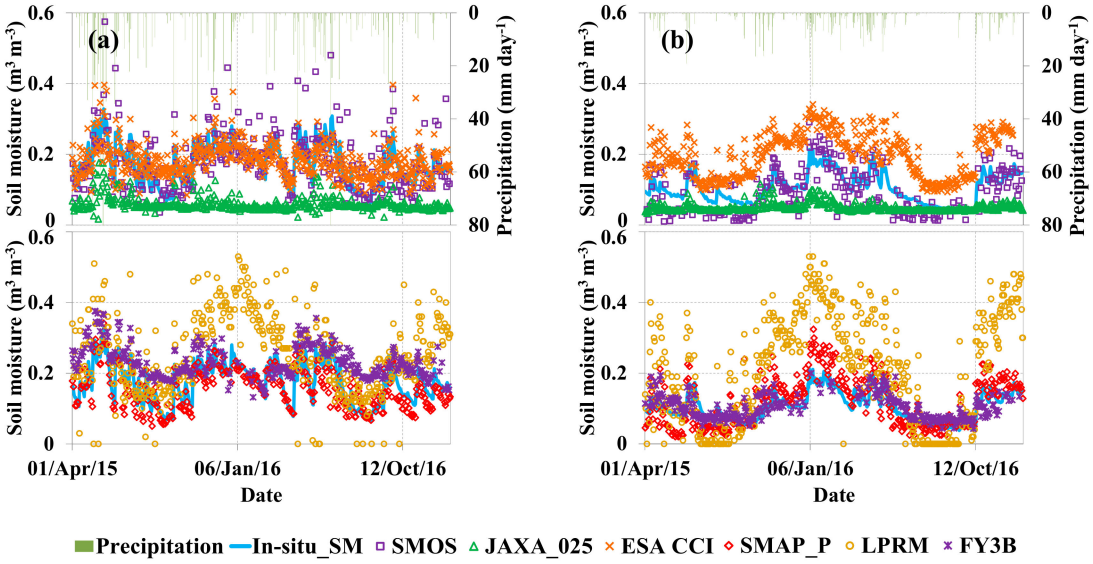


**Figure 3.** Temporal evolution of the station-averaged soil moisture and satellite soil moisture with a spatial resolution of 0.25° for the (**a**) LWW and (**b**) REMEDHUS networks. Soil moisture products are divided into the vertically-oriented panels in (**a**,**b**) for visualization purposes.

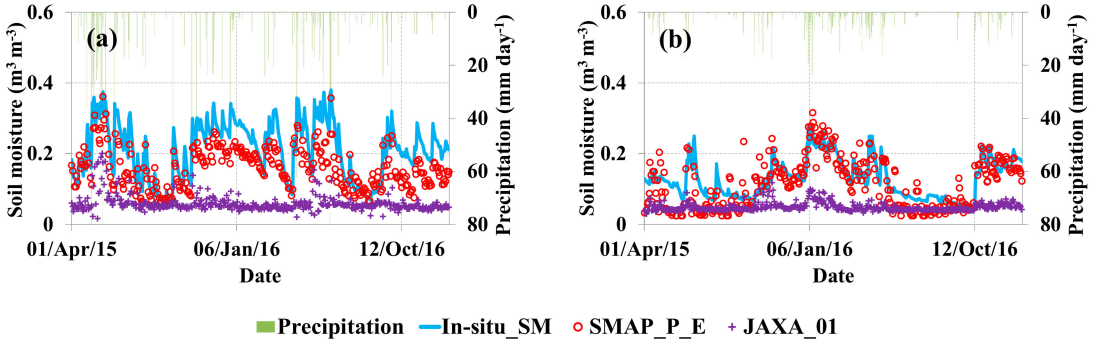


**Figure 4.** Temporal evolution of the station-averaged soil moisture and satellite soil moisture with a spatial resolution of 0.1° for the (**a**) LWW and (**b**) REMEDHUS networks.

As mentioned in Section 3, the soil moisture products at 36 km (i.e., SMAP passive) and 25 km (i.e., SMOS and FY3B) were resampled to the grid resolution of 0.25°, and the soil moisture product at 9 km (i.e., SMAP enhanced passive) was resampled to the grid resolution of 0.1°. The daily station-averaged in-situ observations within the red grid at 0.25° (shown in Figure 1) were selected to assess the accuracy of six products, including the SMAP passive, SMOS, JAXA (0.25°), LPRM, ESA CCI, and FY3B soil moisture products, as displayed in Figure 3. Meanwhile, the blue grid nested to the red grid was used for validating the SMAP enhanced passive and JAXA (0.1°) soil moisture products, as shown in Figure 4.

In the LWW network region, we can see that although both of the SMAP passive and enhanced passive products underestimated the ground soil moisture measurements, with a bias of $-0.018$ $m^3$ $m^{-3}$ and $-0.050$ $m^3$ $m^{-3}$, respectively, these products were superior to other products, with a correlation coefficient higher than 0.87 and an ubRMSE smaller than 0.04 $m^3$ $m^{-3}$, which is well within the mission requirements of 0.04 $m^3$ $m^{-3}$ (ubRMSE). The correlation coefficient of the SMOS product is 0.71, which is also higher than that of JAXA and LPRM. It was observed that SMAP and SMOS could capture the temporal variations of near-surface soil moisture better than JAXA and LPRM. This was consistent with the general expectation that the L-band has a deeper depth of emission layer, and is less susceptible to the influences of vegetation and atmosphere compared to higher frequencies, such as the C-band and the X-band. The ESA CCI soil moisture product showed good agreement with the in-situ measurements in the LWW network, with an ubRMSE value of 0.044 $m^3$ $m^{-3}$, which was smaller than SMOS, LPRM and JAXA. This is in line with the results reported in [16], revealing the effectiveness of merging active and passive soil moisture products to improve the accuracy of a single satellite soil moisture product. Besides, it was observed that the ESA CCI product had the highest number of valid values when compared with other products, which is benefited from combining multiple soil moisture products, including active and passive satellite products, in this region. The JAXA soil moisture products at 0.1° and 0.25° underestimated soil moisture most of the time, with a dry bias of $-0.114$ $m^3$ $m^{-3}$ and $-0.151$ $m^3$ $m^{-3}$, respectively, while the LPRM soil moisture product had a larger dynamic range than in-situ soil moisture, and overestimated soil moisture with a wet bias of 0.091 $m^3$ $m^{-3}$. This was generally in accordance with previous studies, which found that LPRM usually overestimates soil moisture, while JAXA usually underestimates ground measurements [16,61]. Additionally, it can be seen that the JAXA product performs much better at a coarse spatial resolution (0.25°) than at a medium spatial resolution (0.1°), with a lower ubRMSE and RMSE values of 0.050 $m^3$ $m^{-3}$ and 0.125 $m^3$ $m^{-3}$, respectively, and a higher correlation coefficient value of 0.48, which may be due to the oversampling of the AMSR2 brightness temperature. It was observed that the FY3B soil moisture product outperformed other products, except SMAP, with a small ubRMSE of 0.041 $m^3$ $m^{-3}$ and a high correlation coefficient of 0.71. This may be because the FY3B algorithm uses a distinctly different approach to correct the influence of surface roughness, which may be more effective than other satellite soil moisture algorithms in the LWW network region. With the exception of the FY3B algorithm, a common assumption made in the satellite soil moisture algorithms is the global (e.g., LPRM, JAXA and SMOS) or land-cover specific (e.g., SMAP) constant value of surface roughness [16,23,24]. In the LWW network region, rainfall is very frequent, and the statistical properties of surface roughness will change due to the rainfall effects. Consequently, the constant assumption of the surface roughness will inevitably bring errors to the satellite soil moisture retrievals. Additionally, the Taylor diagram was used to provide a comprehensive view of how closely the satellite products matched the ground measurements. As illustrated in Figures 5a and 6a, the variability of the SMAP passive and enhanced passive products, FY3B and ESA CCI were very close to that of the ground measurements, whereas LPRM and SMOS were more variable than the ground measurements, and JAXA (both at 0.25° and 0.1°) showed a lower variability than the in-situ observations.

In the REMEDHUS network region, it was observed that the SMAP enhanced passive, SMOS, and JAXA products still underestimated soil moisture, with a dry bias ($-0.015$ $m^3$ $m^{-3}$, $-0.012$ $m^3$ $m^{-3}$, $-0.055$ $m^3$ $m^{-3}$ respectively) similar to that found in the LWW region. The correlation coefficient of SMAP passive and SMOS products were 0.83, higher than that of the JAXA product (0.60), whereas the ubRMSE value of the JAXA product was 0.035 $m^3$ $m^{-3}$, smaller than that of the SMAP (0.044 $m^3$ $m^{-3}$) and SMOS (0.038 $m^3$ $m^{-3}$) products. It can be seen from Table 2 that the LPRM and ESA CCI products all overestimated soil moisture, with a wet bias of 0.106 $m^3$ $m^{-3}$ and 0.097 $m^3$ $m^{-3}$, respectively, but had slightly higher correlations with the ground measurements when compared with the other satellite products, except for SMAP. However, it was found that the LPRM product showed significantly larger amplitude than the ground soil moisture, and the ubRMSE of the LPRM product was much higher than the other products. The JAXA product at a coarse resolution of 0.25° still outperformed the same product

at 0.1°, which was in line with the results found in the LWW network region. The SMAP enhanced passive product performed better than JAXA at 0.1°, with a higher *R* value and smaller ubRMSE, RMSE, and bias values. Generally, the FY3B exhibited the best performance over the other satellite products in the REMEDHUS network region, with ubRMSE and RMSE values smaller than 0.03 $m^3$ $m^{-3}$, and a relatively higher correlation coefficient value of 0.75, demonstrating the product's great potential to be integrated into the existing long-term soil moisture data record (e.g., the ESA CCI product). In addition, from Figures 5b and 6b, it is seen that the temporal variation of the FY3B product was in accordance with that of the ground observations, whereas the variability of the other satellite products was lower than the in-situ measurements (except the JAXA product).

**Table 1.** Comparison of the Soil Moisture Active Passive (SMAP) passive, Soil Moisture and Ocean Salinity (SMOS), Fengyun-3B (FY3B), Japan Aerospace Exploration Agency (JAXA), and Land Parameter Retrieval Model (LPRM) products at a spatial resolution of 0.25°, and SMAP enhanced passive and JAXA Advanced Microwave Scanning Radiometer 2 (AMSR2) products at a spatial resolution of 0.1°, with in-situ measurements, for the LWW network. The unbiased root mean square error (ubRMSE), root mean square error (RMSE), and bias are in $m^3$ $m^{-3}$, *R* is the correlation coefficient (*p*-value < 0.01), and *N* is the number of samples. Bold data in the table represent the best results concerning each error metric.

| Resolution | Products | *ubRMSE* ($m^3$ $m^{-3}$) | *RMSE* ($m^3$ $m^{-3}$) | *Bias* ($m^3$ $m^{-3}$) | *R* | *N* |
|---|---|---|---|---|---|---|
| 0.25° | SMAP passive | **0.027** | **0.032** | −0.018 | **0.89** | 311 |
| | SMOS | 0.057 | 0.057 | **−0.004** | 0.71 | 328 |
| | FY3B | 0.041 | 0.078 | 0.067 | 0.71 | 311 |
| | JAXA | 0.050 | 0.125 | −0.114 | 0.48 | 478 |
| | LPRM | 0.108 | 0.141 | 0.091 | 0.54 | 464 |
| | ESA CCI | 0.044 | 0.045 | 0.009 | 0.66 | 585 |
| 0.1° | SMAP enhanced passive | 0.040 | 0.064 | −0.050 | 0.88 | 312 |
| | JAXA | 0.073 | 0.168 | −0.151 | 0.41 | 468 |

**Table 2.** Comparison of the SMAP passive, SMOS, FY3B, JAXA, and LPRM products at a spatial resolution of 0.25°, and the SMAP enhanced passive and JAXA AMSR2 products at a spatial resolution of 0.1°, with in-situ measurements, for the REMEDHUS network. The ubRMSE, RMSE, and bias are in $m^3$ $m^{-3}$, *R* is the correlation coefficient (*p*-value < 0.01), and *N* is the number of samples. Bold data in the table represent the best results concerning each error metric.

| Resolution | Products | *ubRMSE* ($m^3$ $m^{-3}$) | *RMSE* ($m^3$ $m^{-3}$) | *Bias* ($m^3$ $m^{-3}$) | *R* | *N* |
|---|---|---|---|---|---|---|
| 0.25° | SMAP passive | 0.044 | 0.047 | 0.016 | **0.83** | 348 |
| | SMOS | 0.038 | 0.040 | −0.012 | **0.83** | 236 |
| | FY3B | **0.025** | **0.027** | **0.009** | 0.75 | 325 |
| | JAXA | 0.035 | 0.065 | −0.055 | 0.60 | 538 |
| | LPRM | 0.121 | 0.161 | 0.106 | 0.82 | 518 |
| | ESA CCI | 0.036 | 0.104 | 0.097 | **0.83** | 464 |
| 0.1° | SMAP enhanced passive | 0.039 | 0.042 | −0.015 | **0.83** | 332 |
| | JAXA | 0.046 | 0.091 | −0.079 | 0.61 | 517 |

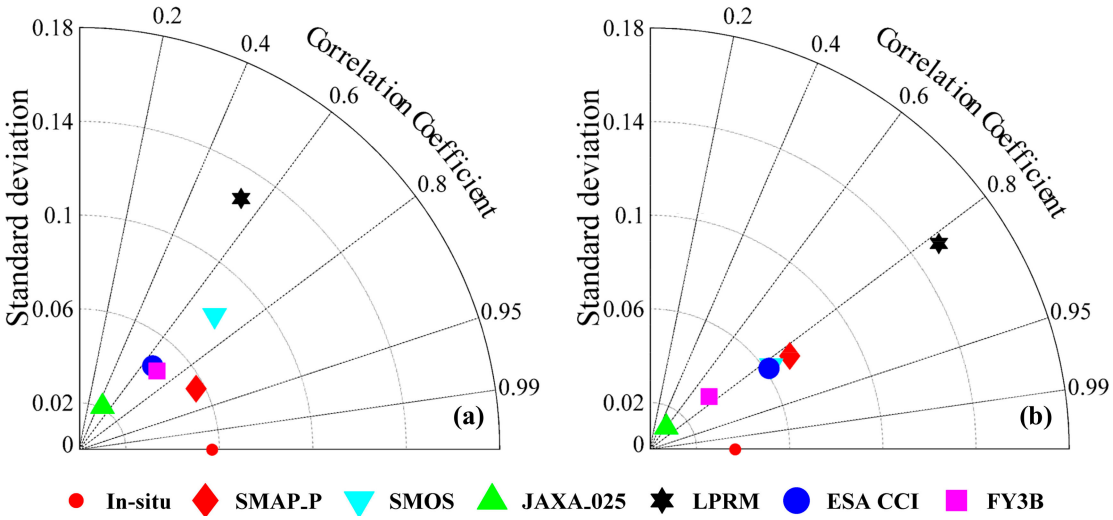


**Figure 5.** Taylor diagram illustrating the statistics of the comparison between station-averaged soil moisture and satellite soil moisture, with a spatial resolution of 0.25°, for the (**a**) LWW and (**b**) REMEDHUS networks.

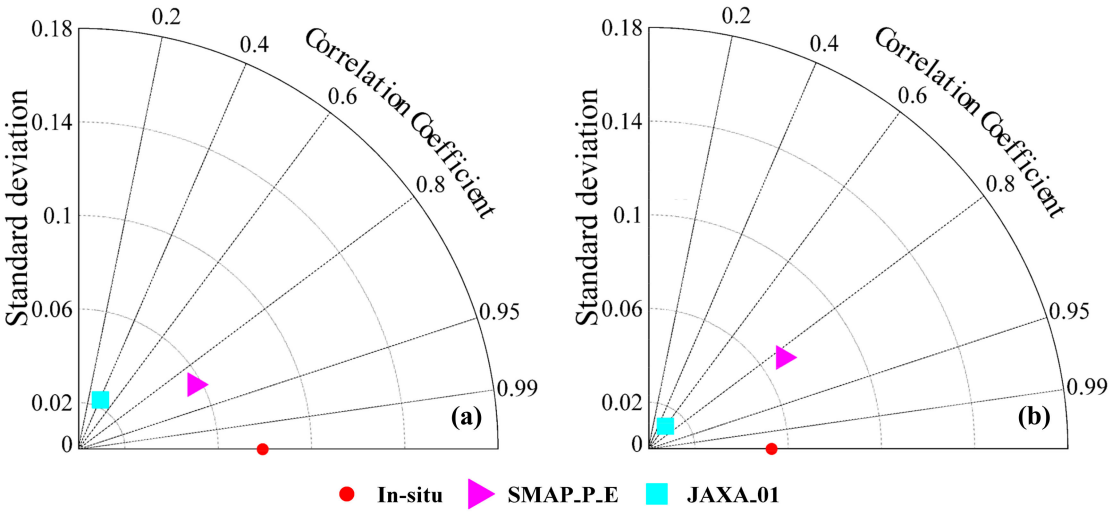


**Figure 6.** Taylor diagram illustrating the statistics of the comparison between station-averaged soil moisture and satellite soil moisture, with a spatial resolution of 0.1°, for the (**a**) LWW and (**b**) REMEDHUS networks.

## 5. Discussion

Apart from the examination of the accuracy of the eight remotely-sensed soil moisture products, we also investigate some possible factors that might lead to the different performance of the soil moisture products. These include assessing the accuracy of satellite surface temperature using station-averaged ground measurements, as shown in Figure 7, and examining the temporal behavior of the satellite-derived vegetation optical depth and vegetation water content, as shown in Figure 8.

### *5.1. Assessment of Satellite Surface Temperature Data*

Many factors impact the validation accuracy of satellite soil moisture products, including (1) the uncertainties originating from the well-known horizontal and vertical mismatch between in-situ soil moisture and satellite observations (commonly, the effective soil moisture sampling depth at the L-band and C/X-band is 0–3 cm and 0–1 cm, respectively, and also depends on soil moisture [16,22], while the

ground soil moisture is measured at 5 cm); (2) the possible errors in ground measurements; (3) the effects of RFI; and (4) the inaccurate correction of the perturbing factors (e.g., surface temperature, vegetation, and surface roughness) in the soil moisture retrieval algorithm [23]. In contrast to active microwave backscatter, which is nearly unaffected by surface temperature, the passive observations are heavily controlled by temperature. Thus, the effects of surface temperature must be eliminated for reliable soil moisture retrievals [10]. In SMAP and SMOS soil moisture retrieval algorithms, the surface temperatures are all derived from model simulations. The SMAP surface temperature is predicted from the NASA GEOS-5 model, and SMOS surface temperature is obtained from the ECMWF model. In contrast, in LPRM, the surface temperature is retrieved separately from the 36.5 GHz V-pol brightness temperature. In the FY3B algorithm, a similar approach to LPRM is adopted to correct the effects of surface temperature, but the surface temperature data is not provided at present. For the JAXA algorithm, the PI and ISW are applied to minimize the effects of surface temperature to retrieve soil moisture. Therefore, in this section, we examine the accuracy of the surface temperature provided by the SMAP, SMOS and AMSR2 (LPRM) products, shown in Figure 7. It should be noted that in the SMOS algorithm, a two-layer algorithm [9] is adopted to calculate the effective soil temperature, which can eliminate the influence of temperature more effectively. However, in the SMOS CATDS product, only the soil temperature of the first layer from ECMWF (i.e., Temp_STL1) is provided. In our study, the SMOS surface temperature ancillary data we examined is the Temp_STL1 product, which is not the actual soil effective temperature used in the SMOS algorithm.

It was observed that the SMAP and SMOS surface temperatures were closer to the 1:1 line when compared with the LPRM surface temperature, indicating that the temperatures estimated by the forecast models were more accurate than the satellite derived temperatures in the two network regions. As seen from Tables 3 and 4, SMAP exhibits the highest absolute accuracy among the four products, with the lowest RMSE and ubRMSE values, followed by SMOS and LPRM. Theoretically, an underestimation of surface temperature will result in an overestimation of soil emissivity, further leading to an underestimation of soil moisture. From Tables 3 and 4, it was seen that the SMAP and SMOS surface temperature showed dry bias in the two network regions, which is in accordance with the general underestimation of SMAP and SMOS soil moisture products found in Section 4. Therefore, the underestimated surface temperatures may be one factor that results in a dry bias of SMAP and SMOS soil moisture products. Additionally, though the LPRM surface temperature also showed a dry bias, which is in line with [10] at nighttime, the LPRM soil moisture always overestimated soil moisture, with a wet bias larger than 0.09 $m^3$ $m^{-3}$, in both network regions. Consequently, the overestimation of LPRM soil moisture was not caused by its surface temperature retrievals.

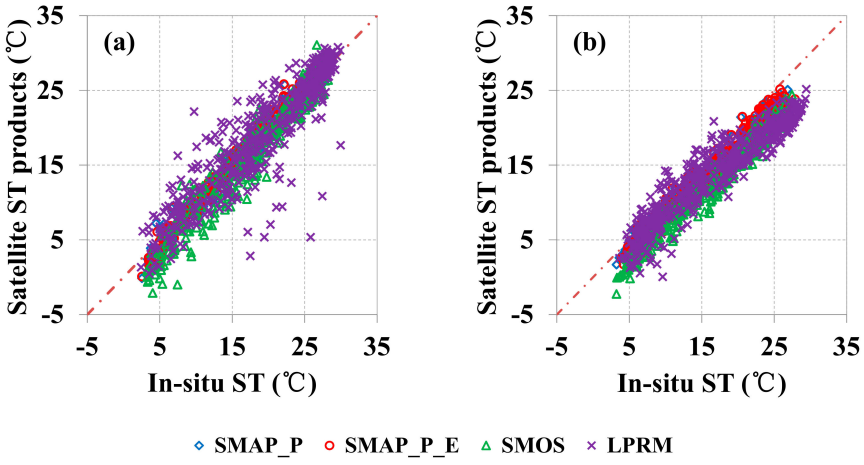


**Figure 7.** Scatterplot comparison of the station-averaged surface temperature and satellite surface temperature ancillary data for the (**a**) LWW and (**b**) REMEDHUS network regions.

**Table 3.** Comparison of the SMAP passive, SMAP enhanced passive, SMOS, and LPRM surface temperature ancillary data, with in-situ measurements, for the LWW network region. The ubRMSE, RMSE, and bias are in K, while *R* is the correlation coefficient (*p*-value < 0.01), and *N* is the number of samples. Bold data in the table represent the best results concerning each error metric.

| Products | *ubRMSE* (K) | *RMSE* (K) | *Bias* (K) | *R* | *N* |
|---|---|---|---|---|---|
| SMAP passive | 1.062 | 1.153 | −0.449 | **0.99** | 315 |
| SMAP enhanced passive | **1.030** | **1.031** | **−0.047** | **0.99** | 314 |
| SMOS * | 2.035 | 2.413 | −1.297 | 0.97 | 333 |
| LPRM | 3.337 | 3.338 | −0.088 | 0.91 | 464 |

* The SMOS surface temperature ancillary data evaluated in the study was the temperature of the first layer of soil from the European Centre for Medium-Range Weather Forecasts (ECMWF) (Temp_STL1).

**Table 4.** Comparison of the SMAP passive (SMAP_P), SMAP enhanced passive (SMAP_P_E), SMOS, and LPRM surface temperature ancillary data, with in-situ measurements, for the REMEDHUS network region. The ubRMSE, RMSE, and bias are in K, *R* is the correlation coefficient (*p*-value < 0.01), and *N* is the number of samples. Bold data in the table represent the best results concerning each error metric.

| Products | *ubRMSE* (K) | *RMSE* (K) | *Bias* (K) | *R* | *N* |
|---|---|---|---|---|---|
| SMAP passive | **1.029** | **2.194** | **−1.937** | **0.99** | 348 |
| SMAP enhanced passive | 1.110 | 2.315 | −2.032 | **0.99** | 339 |
| SMOS * | 1.440 | 3.903 | −3.628 | 0.98 | 347 |
| LPRM | 2.653 | 3.833 | −2.767 | 0.94 | 516 |

* The SMOS surface temperature ancillary data evaluated in the study is the temperature of the first layer of soil from ECMWF (Temp_STL1).

### *5.2. Temporal Behavior of Satellite Vegetation Optical Depth*

The vegetation canopy exerts significant effects on the soil-emitted energy. Vegetation not only attenuates signals from soil surfaces, but also emits radiation itself, leading to a reduced sensitivity of brightness temperature to soil moisture. Accordingly, the influence of vegetation must be corrected accurately before achieving reliable soil moisture estimations. Commonly, the effects of vegetation are mainly represented by the vegetation optical depth (i.e., $\tau_c$). In the current SMAP passive baseline soil moisture algorithm, the VWC is considered as a good proxy to calculate the vegetation optical depth. However, obtaining the real VWC measurements at a global scale is practically impossible. To solve this problem, the VWC is empirically estimated, by using a global, 13-year (2000–2013) MODIS NDVI climatology in the SMAP passive soil moisture algorithm. The FY3B and JAXA algorithms also adopt a similar approach to SMAP to correct the effects of vegetation, but their vegetation-related products are not currently released to the public. In the LPRM and SMOS algorithms, vegetation optical depth is estimated simultaneously with soil moisture. For LPRM, the PI is applied to obtain vegetation optical depth, to avoid a reliance on additional vegetation datasets. For SMOS, vegetation optical depth is retrieved from multi-angular brightness temperature observations. In contrast to SMOS and LPRM, the vegetation optical depth of SMAP is estimated from the VWC, which is calculated using the MODIS NDVI climatology.

In this study, we examined the temporal variations of the vegetation optical depth derived from SMAP, SMOS, and LPRM, as well as the VWC extracted from SMAP passive soil moisture product, as shown in Figure 8. It can be observed that the LPRM $\tau_c$ had a much larger value than SMAP and SMOS $\tau_c$. A high $\tau_c$ value indicates a low transmissivity of the vegetation, which may lead to low soil emissivity. It is known that soil emissivity generally decreases as soil moisture increases. Thus, it may be possibly deduced that the high LPRM soil moisture is caused by the high estimated $\tau_c$ value. Additionally, it can be seen that the SMAP $\tau_c$ shows much smoother variation than SMOS and LPRM during the entire period. The SMOS $\tau_c$ seems noisy, leading to a very large dynamic range of $\tau_c$ (>0.4) in the two network regions. In general, an increase of vegetation biomass leads to an increase of

vegetation optical depth. Thus, in theory there should be a positive correlation between $\tau_c$ and VWC. However, SMOS $\tau_c$ does not show significant correlations with VWC, with a correlation coefficient of 0.26 and 0.03 in the LWW and REMEDHUS network regions, respectively. In contrast, LPRM $\tau_c$ shows a good response to VWC, with a correlation coefficient of 0.39 in the LWW network region and 0.68 in the REMEDHUS network region. Meanwhile, it is worth mentioning that the SMAP-derived VWC is not the real vegetation water content seen by the microwave. This is because the optical wavelength is much smaller than the microwave, and can only represent the information of a very thin layer of the vegetation canopy. In contrast, the microwave is able to penetrate vegetation to some extent, and thus contains some information of the vegetation stem and branches. This is more evident at the L-band than at the C-band and X-band, leading to the lower correlation of the L-band with NDVI VWC than that of the C-band and X-band. The SMOS-retrieved $\tau_c$ exhibits a day-to-day variability, which is not consistent with the actual changes in the vegetation. This is in line with the finding reported in [19]. Thus, the variation in SMOS $\tau_c$ should be one error source in the SMOS soil moisture product. A new vegetation parameterization scheme is expected to be incorporated into the SMOS algorithm, in order to improve the accuracy of SMOS soil moisture retrievals in the future.

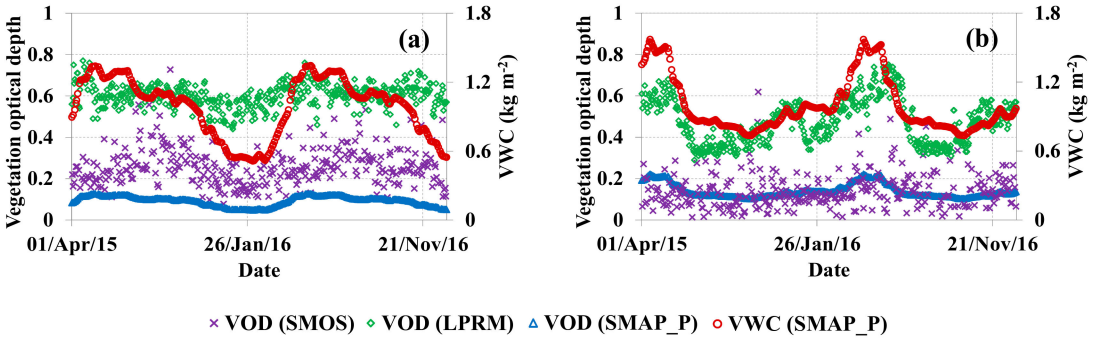


**Figure 8.** Temporal evolution of satellite-estimated vegetation optical depth (VOD) and vegetation water content (VWC) for the (**a**) LWW and (**b**) REMEDHUS network regions.

## 6. Conclusions

Knowledge on the accuracy and reliability of satellite soil moisture products is essential for their improvement as well as their utilization in scientific studies and applications. This study examined the performance of eight satellite-based soil moisture products, including the SMAP passive, the SMAP enhanced passive, SMOS, JAXA AMSR2, LPRM AMSR2, ESA CCI, and FY3B soil moisture products, using two representative dense networks (LWW and REMEDHUS) at two typical spatial resolutions, i.e., a coarse resolution of 0.25° and a medium resolution of 0.1°.

Overall, the SMAP passive and enhanced passive soil moisture products are superior to other products, with a correlation coefficient higher than 0.87 and an ubRMSE smaller than 0.04 $m^3$ $m^{-3}$ in the LWW network region. Meanwhile, it was found that the SMAP and SMOS generally underestimate the in-situ soil moisture measurements, except for the SMAP passive at the REMEDHUS network region, with a wet bias of 0.016 $m^3$ $m^{-3}$, whereas LPRM overestimated the ground soil moisture with much greater amplitude than the in-situ measurements (bias > 0.09 $m^3$ $m^{-3}$). The SMAP and SMOS surface temperature showed dry bias in the two network regions, which may have been one of the reasons for the underestimation of soil moisture. The surface temperature of LPRM also showed a dry bias (−0.088 K for LWW and −2.767 K for REMEDHUS), and thus was not the reason for the overestimation of LPRM soil moisture. Compared with LPRM, the SMAP and SMOS surface temperatures were closer to the 1:1 line, illustrating that the temperatures estimated by the forecast models were more accurate than temperatures retrieved from satellite observations in the two network regions. SMAP (passive and enhanced passive) surface temperature shows the highest absolute accuracy among the four products, with the lowest RMSE (<2.4 K) and ubRMSE (<1.2 K) values,

followed by SMOS, and LPRM. The variability of SMOS-retrieved $\tau_c$ was not consistent with the actual changes in the vegetation, and thus the SMOS $\tau_c$ should be one error source in the SMOS soil moisture product. The performance of the JAXA product was much better at a coarse spatial resolution (0.25°) than at a medium spatial resolution (0.1°) with a higher correlation coefficient value and a lower ubRMSE and RMSE value, but both of these two products underestimated the soil moisture most of the time (bias < $-0.05$ $m^3$ $m^{-3}$). Furthermore, the SMAP passive enhanced soil moisture product generally outperformed the JAXA product at the spatial resolution of 0.1°. The ESA CCI soil moisture product showed good agreement with the in-situ soil moisture, with favorable ubRMSE values of 0.044 $m^3$ $m^{-3}$ and 0.036 $m^3$ $m^{-3}$ in the LWW and REMEDHUS network regions, respectively, which were smaller than the SMOS and LPRM products, revealing the effectiveness of merging active and passive soil moisture products. It is worthwhile noting that the Chinese FY3B soil moisture product exhibited a very good performance in both the LWW and REMEDHUS network regions, with a small ubRMSE of 0.041 $m^3$ $m^{-3}$ and 0.025 $m^3$ $m^{-3}$, respectively, and high correlation coefficients of 0.71 and 0.75, respectively. The temporal variation of the FY3B product was also in accordance with that of ground observations. This may have been caused by the fact that FY3B algorithm uses a distinctly different approach to correct the influence of surface roughness, which may have been more effective than other satellite soil moisture algorithms in the two study areas. In summary, our study reveals the good quality of the SMAP and FY3B soil moisture products, demonstrating the great potential to integrate them into the existing long-term soil moisture data record, i.e., the ESA CCI product, in order to form a more reliable and useful product.

**Acknowledgments:** The work was supported by the Open Research Fund of Key Laboratory of Digital Earth Science, Institute of Remote Sensing and Digital Earth, Chinese Academy of Sciences under Grant 2016LDE003, the National Natural Science Foundation of China under Grant 41601371, 41531175 and 41471430, the 13th Five-Year Plan of Civil Aerospace Technology Advanced Research Projects (2016, NO. 1299). Jiangyuan Zeng was supported by the Youth Innovation Promotion Association CAS. The authors would like to thank Nemesio Rodriguez-Fernandez and the four reviewers for their helpful reviews and suggestions, and the NSIDC, CATDS, CNES, CNSMC, GES DISC, JAXA and ESA for providing the satellite soil moisture products, and the U.S. Department of Agriculture Agricultural Research Service and the ISMN for providing the in-situ data.

**Author Contributions:** Jiangyuan Zeng conceived and designed the research and analyzed the results; Chenyang Cui performed the experiment under the supervision of Jiangyuan Zeng; Chenyang Cui and Jiangyuan Zeng wrote the paper; Jia Xu, Kun-Shan Chen, and Hui Lu supported the discussion and interpretation of the results, Xiaojing Bai, Quan Chen, and Tianjie Zhao gave comments and modified the manuscript. All authors contributed to the editing of the manuscript.

**Conflicts of Interest:** The authors declare no conflict of interest.

## References

1. Wagner, W.; Hahn, S.; Kidd, R.; Melzer, T.; Bartalis, Z.; Hasenauer, S.; Figa-Saldaña, J.; De Rosnay, P.; Jann, A.; Schneider, S.; et al. The ASCAT soil moisture product: A review of its specifications, validation results, and emerging applications. *Meteorol. Z.* **2013**, *22*, 5–33. [CrossRef]
2. Njoku, E.G.; Jackson, T.J.; Lakshmi, V.; Chan, T.K.; Nghiem, S.V. Soil moisture retrieval from AMSR-E. *IEEE Trans. Geosci. Remote Sens.* **2003**, *41*, 215–229. [CrossRef]
3. Imaoka, K.; Maeda, T.; Kachi, M.; Kasahara, M.; Ito, N.; Nakagawa, K. Status of AMSR2 instrument on GCOM-W1. *Proc. SPIE* **2012**, *8528*, 852815. [CrossRef]
4. Kerr, Y.H.; Waldteufel, P.; Wigneron, J.P.; Delwart, S.; Cabot, F.; Boutin, J.; Escorihuela, M.J.; Font, J.; Reul, N.; Gruhier, C.; et al. The SMOS mission: New tool for monitoring key elements of the global water cycle. *Proc. IEEE* **2010**, *98*, 666–687. [CrossRef]
5. Entekhabi, D.; Njoku, E.G.; O'Neill, P.E.; Kellogg, K.H.; Crow, W.T.; Edelstein, W.N.; Entin, J.K.; Goodman, S.D.; Jackson, T.J.; Johnson, J.; et al. The soil moisture active passive (SMAP) mission. *Proc. IEEE* **2010**, *98*, 704–716. [CrossRef]
6. Wagner, W.; Lemoine, G.; Rott, H. A method for estimating soil moisture from ERS scatterometer and soil data. *Remote Sens. Environ.* **1999**, *70*, 191–207. [CrossRef]

7. Wigneron, J.P.; Jackson, T.J.; O'neill, P.; De Lannoy, G.; De Rosnay, P.; Walker, J.P.; Ferrazzoli, P.; Mironov, V.; Bircher, S.; Grant, J.P.; et al. Modelling the passive microwave signature from land surfaces: A review of recent results and application to the L-band SMOS & SMAP soil moisture retrieval algorithms. *Remote Sens. Environ.* **2017**, *192*, 238–262.
8. Naeimi, V.; Scipal, K.; Bartalis, Z.; Hasenauer, S.; Wagner, W. An improved soil moisture retrieval algorithm for ERS and METOP scatterometer observations. *IEEE Trans. Geosci. Remote Sens.* **2009**, *47*, 1999–2013. [CrossRef]
9. Kerr, Y.H.; Waldteufel, P.; Richaume, P.; Wigneron, J.P.; Ferrazzoli, P.; Mahmoodi, A.; Bitar, A.A.; Cabot, F.; Gruhier, C.; Juglea, S.E.; et al. The SMOS soil moisture retrieval algorithm. *IEEE Trans. Geosci. Remote Sens.* **2012**, *50*, 1384–1403. [CrossRef]
10. Zeng, J.; Li, Z.; Chen, Q.; Bi, H. Method for soil moisture and surface temperature estimation in the Tibetan Plateau using spaceborne radiometer observations. *IEEE Geosci. Remote Sens. Lett.* **2015**, *12*, 97–101. [CrossRef]
11. Jackson, T.J., III. Measuring surface soil moisture using passive microwave remote sensing. *Hydrol. Process.* **1993**, *7*, 139–152. [CrossRef]
12. Owe, M.; de Jeu, R.; Holmes, T. Multisensor historical climatology of satellite-derived global land surface moisture. *J. Geophys. Res. Earth Surf.* **2008**, *113*. [CrossRef]
13. Yang, J.; Zhang, P.; Lu, N.; Yang, Z.; Shi, J.; Dong, C. Improvements on global meteorological observations from the current Fengyun 3 satellites and beyond. *Int. J. Digit. Earth* **2012**, *5*, 251–265. [CrossRef]
14. Dorigo, W.; Wagner, W.; Albergel, C.; Albrecht, F.; Balsamo, G.; Brocca, L.; Chung, D.; Ertl, M.; Forkel, M.; Gruber, A.; et al. ESA CCI Soil Moisture for improved Earth system understanding: State-of-the art and future directions. *Remote Sens. Environ.* **2017**, *203*, 185–215. [CrossRef]
15. Parinussa, R.M.; Wang, G.; Holmes, T.R.H.; Liu, Y.Y.; Dolman, A.J.; De Jeu, R.A.M.; Jiang, T.; Zhang, P.; Shi, J. Global surface soil moisture from the Microwave Radiation Imager onboard the Fengyun-3B satellite. *Int. J. Remote Sens.* **2014**, *35*, 7007–7029. [CrossRef]
16. Zeng, J.; Li, Z.; Chen, Q.; Bi, H.; Qiu, J.; Zou, P. Evaluation of remotely sensed and reanalysis soil moisture products over the Tibetan Plateau using in-situ observations. *Remote Sens. Environ.* **2015**, *163*, 91–110. [CrossRef]
17. Montzka, C.; Bogena, H.R.; Zreda, M.; Monerris, A.; Morrison, R.; Muddu, S.; Vereecken, H. Validation of spaceborne and modelled surface soil moisture products with cosmic-ray neutron probes. *Remote Sens.* **2017**, *9*, 103. [CrossRef]
18. Albergel, C.; De Rosnay, P.; Gruhier, C.; Muñoz-Sabater, J.; Hasenauer, S.; Isaksen, L.; Kerr, Y.; Wagner, W. Evaluation of remotely sensed and modelled soil moisture products using global ground-based in-situ observations. *Remote Sens. Environ.* **2012**, *118*, 215–226. [CrossRef]
19. Su, Z.; Wen, J.; Dente, L.; Velde, R.; Wang, L.; Ma, Y.; Yang, K.; Hu, Z. The Tibetan Plateau observatory of plateau scale soil moisture and soil temperature (Tibet-Obs) for quantifying uncertainties in coarse resolution satellite and model products. *Hydrol. Earth Syst. Sci.* **2011**, *15*, 2303–2316. [CrossRef]
20. Jackson, T.J.; Cosh, M.H.; Bindlish, R.; Starks, P.J.; Bosch, D.D.; Seyfried, M.; Goodrich, D.C.; Moran, M.S.; Du, J. Validation of advanced microwave scanning radiometer soil moisture products. *IEEE Trans. Geosci. Remote Sens.* **2010**, *48*, 4256–4272. [CrossRef]
21. Jackson, T.J.; Bindlish, R.; Cosh, M.H.; Zhao, T.; Starks, P.J.; Bosch, D.D.; Seyfried, M.; Moran, M.S.; Goodrich, D.C.; Kerr, Y.H.; et al. Validation of Soil Moisture and Ocean Salinity (SMOS) soil moisture over watershed networks in the US. *IEEE Trans. Geosci. Remote Sens.* **2012**, *50*, 1530–1543. [CrossRef]
22. Al-Yaari, A.; Wigneron, J.P.; Ducharne, A.; Kerr, Y.; De Rosnay, P.; De Jeu, R.; Govind, A.; Al Bitar, A.; Albergel, C.; Muñoz-Sabater, J.; et al. Global-scale evaluation of two satellite-based passive microwave soil moisture datasets (SMOS and AMSR-E) with respect to Land Data Assimilation System estimates. *Remote Sens. Environ.* **2014**, *149*, 181–195. [CrossRef]
23. Zeng, J.; Chen, K.S.; Bi, H.; Chen, Q. A preliminary evaluation of the SMAP radiometer soil moisture product over United States and Europe using ground-based measurements. *IEEE Trans. Geosci. Remote Sens.* **2016**, *54*, 4929–4940. [CrossRef]
24. Chan, S.K.; Bindlish, R.; O'Neill, P.E.; Njoku, E.; Jackson, T.; Colliander, A.; Chen, F.; Burgin, M.; Dunbar, S.; Piepmeier, J.; et al. Assessment of the SMAP passive soil moisture product. *IEEE Trans. Geosci. Remote Sens.* **2016**, *54*, 4994–5007. [CrossRef]

25. Colliander, A.; Jackson, T.J.; Bindlish, R.; Chan, S.; Das, N.; Kim, S.B.; Cosh, M.H.; Dunbar, R.S.; Dang, L.; Pashaian, L.; et al. Validation of SMAP surface soil moisture products with core validation sites. *Remote Sens. Environ.* **2017**, *191*, 215–231. [CrossRef]
26. Anam, R.; Chishtie, F.; Ghuffar, S.; Qazi, W.; Shahis, I. Inter-comparison of SMOS and AMSR-E soil moisture products during flood years (2010–2011) over Pakistan. *Eur. J. Remote Sens.* **2017**, *50*, 442–451. [CrossRef]
27. Zhuo, L.; Han, D. Hydrological evaluation of satellite soil moisture data in two basins of different climate and vegetation density conditions. *Adv. Meteorol.* **2017**. [CrossRef]
28. Ray, R.L.; Fares, A.; He, Y.; Temimi, M. Evaluation and Inter-comparison of satellite soil moisture products using in situ observations over Texas. *Water* **2017**, *9*, 372. [CrossRef]
29. Jackson, T.J.; Le Vine, D.M.; Hsu, A.Y.; Oldak, A.; Starks, P.J.; Swift, C.T.; Isham, J.D.; Haken, M. Soil moisture mapping at regional scales using microwave radiometry: The Southern Great Plains Hydrology Experiment. *IEEE Trans. Geosci. Remote Sens.* **1999**, *37*, 2136–2151. [CrossRef]
30. Sanchez, N.; Martínez-Fernández, J.; Scaini, A.; Perez-Gutierrez, C. Validation of the SMOS L2 soil moisture data in the REMEDHUS network (Spain). *IEEE Trans. Geosci. Remote Sens.* **2012**, *50*, 1602–1611. [CrossRef]
31. Kornelsen, K.C.; Cosh, M.H.; Coulibaly, P. Potential of bias correction for downscaling passive microwave and soil moisture data. *J. Geophys. Res.* **2015**, *120*, 6460–6479. [CrossRef]
32. Dorigo, W.A.; Wagner, W.; Hohensinn, R.; Hahn, S.; Paulik, C.; Xaver, A.; Gruber, A.; Drusch, M.; Mecklenburg, S.; Van Oevelen, P.; et al. The International Soil Moisture Network: A data hosting facility for global in-situ soil moisture measurements. *Hydrol. Earth Syst. Sci.* **2011**, *15*, 1675–1698. [CrossRef]
33. Castro, J.; Zamora, R.; Hódar, J.A.; Gómez, J.M. Seedling establishment of a boreal tree species (*Pinus sylvestris*) at its southernmost distribution limit: Consequences of being in a marginal Mediterranean habitat. *J. Ecol.* **2004**, *92*, 266–277. [CrossRef]
34. Ceballos, A.; Martínez-Fernández, J.; Luengo-Ugidos, M.Á. Analysis of rainfall trends and dry periods on a pluviometric gradient representative of Mediterranean climate in the Duero Basin, Spain. *J. Arid Environ.* **2004**, *58*, 215–233. [CrossRef]
35. Wagner, W.; Pathe, C.; Doubkova, M.; Sabel, D.; Bartsch, A.; Hasenauer, S.; Blöschl, G.; Scipal, K.; Martínez-Fernández, J.; Löw, A. Temporal stability of soil moisture and radar backscatter observed by the Advanced Synthetic Aperture Radar (ASAR). *Sensors* **2008**, *8*, 1174–1197. [CrossRef] [PubMed]
36. Piles, M.; Sánchez, N.; Vall-llossera, M.; Camps, A.; Martínez-Fernández, J.; Martínez, J.; González-Gambau, V. A downscaling approach for SMOS land observations: Evaluation of high-resolution soil moisture maps over the Iberian Peninsula. *IEEE J. Sel. Top. Appl. Earth Obs.* **2014**, *7*, 3845–3857. [CrossRef]
37. Sánchez-Ruiz, S.; Piles, M.; Sánchez, N.; Martínez-Fernández, J.; Vall-llossera, M.; Camps, A. Combining SMOS with visible and near/shortwave/thermal infrared satellite data for high resolution soil moisture estimates. *J. Hydrol.* **2014**, *516*, 273–283. [CrossRef]
38. Sánchez, N.; Martínez-Fernández, J.; Calera, A.; Torres, E.; Pérez-Gutiérrez, C. Combining remote sensing and in-situ soil moisture data for the application and validation of a distributed water balance model (HIDROMORE). *Agric. Water Manag.* **2010**, *98*, 69–78. [CrossRef]
39. Choudhury, B.J.; Schmugge, T.J.; Chang, A.; Newton, R.W. Effect of surface roughness on the microwave emission from soils. *J. Geophys. Res. Oceans* **1979**, *84*, 5699–5706. [CrossRef]
40. Mironov, V.L.; Kosolapova, L.G.; Fomin, S.V. Physically and mineralogically based spectroscopic dielectric model for moist soils. *IEEE Trans. Geosci. Remote Sens.* **2009**, *47*, 2059–2070. [CrossRef]
41. O'Neill, P.E.; Chan, S.; Njoku, E.; Jackson, T.J.; Bindlish, R. *Algorithm Theoretical Basis Document (ATBD): L2/3_SM_P, Nat. Aeronaut. Space Admin*; Jet Propulsion Lab.: Pasadena, CA, USA, 2015.
42. Chaubell, J.; Yueh, S.; Entekhabi, D.; Peng, J. Resolution enhancement of SMAP radiometer data using the Backus Gilbert optimum interpolation technique. In Proceedings of the 2016 IEEE International Geoscience and Remote Sensing Symposium, Beijing, China, 10–15 July 2016; pp. 284–287.
43. Poe, G.A. Optimum interpolation of imaging microwave radiometer data. *IEEE Trans. Geosci. Remote Sens.* **1990**, *28*, 800–810. [CrossRef]
44. Chan, S. *Enhanced Level 3 Passive Soil Moisture Product Specification Document*; Jet Propulsion Lab., California Inst. Technol.: Pasadena, CA, USA, 2016.
45. De Jeu, R.A.M. Retrieval of Land Surface Parameters Using Passive Microwave Remote Sensing. Ph.D. Thesis, Vrije Universiteit Amsterdam, Amsterdam, the Netherlands, 2003.

46. Jackson, T.J.; Schmugge, T.J. Vegetation effects on the microwave emission of soils. *Remote Sens. Environ.* **1991**, *36*, 203–212. [CrossRef]
47. Shi, J.; Jiang, L.; Zhang, L.; Chen, K.S.; Wigneron, J.P.; Chanzy, A. A parameterized multifrequency-polarization surface emission model. *IEEE Trans. Geosci. Remote Sens.* **2005**, *43*, 2831–2841.
48. Zeng, J.; Chen, K.S.; Bi, H.; Zhao, T.; Yang, X. A comprehensive analysis of rough soil surface scattering and emission predicted by AIEM with comparison to numerical simulations and experimental measurements. *IEEE Trans. Geosci. Remote Sens.* **2017**, *55*, 1696–1708. [CrossRef]
49. Shi, J.; Jiang, L.; Zhang, L.; Chen, K.S.; Wigneron, J.P.; Chanzy, A.; Jackson, T.J. Physically based estimation of bare-surface soil moisture with the passive radiometers. *IEEE Trans. Geosci. Remote Sens.* **2006**, *44*, 3145–3153. [CrossRef]
50. Wigneron, J.P.; Kerr, Y.; Waldteufel, P.; Saleh, K.; Escorihuela, M.J.; Richaume, P.; Ferrazzoli, P.; De Rosnay, P.; Gurney, R.; Calvet, J.C.; et al. L-band microwave emission of the biosphere (L-MEB) model: Description and calibration against experimental data sets over crop fields. *Remote Sens. Environ.* **2007**, *107*, 639–655. [CrossRef]
51. Lievens, H.; Tomer, S.K.; Al Bitar, A.; De Lannoy, G.J.M.; Drusch, M.; Dumedah, G.; Hendricks Franssen, H.J.; Kerr, Y.H.; Martens, B.; Pan, M.; et al. SMOS soil moisture assimilation for improved hydrologic simulation in the Murray Darling Basin, Australia. *Remote Sens. Environ.* **2015**, *168*, 146–162. [CrossRef]
52. Koike, T.; Nakamura, Y.; Kaihotsu, I.; Davaa, G.; Matsuura, N.; Tamagawa, K.; Fujii, H. Development of an advanced microwave scanning radiometer (AMSR-E) algorithm for soil moisture and vegetation water content. *J. Hydraul. Eng. ASCE* **2004**, *48*, 217–222. [CrossRef]
53. Holmes, T.R.H.; De Jeu, R.A.M.; Owe, M.; Dolman, A.J. Land surface temperature from Ka band (37 GHz) passive microwave observations. *J. Geophys. Res. Atmos.* **2009**, *114*. [CrossRef]
54. Li, L.; Njoku, E.G.; Im, E.; Chang, P.S.; Germain, K.S. A preliminary survey of radio-frequency interference over the US in Aqua AMSR-E data. *IEEE Trans. Geosci. Remote Sens.* **2004**, *42*, 380–390. [CrossRef]
55. Njoku, E.G.; Ashcroft, P.; Chan, T.K.; Li, L. Global survey and statistics of radio-frequency interference in AMSR-E land observations. *IEEE Trans. Geosci. Remote Sens.* **2005**, *43*, 938–947. [CrossRef]
56. Liu, Y.Y.; Dorigo, W.A.; Parinussa, R.M.; De Jeu, R.A.M.; Wagner, W.; McCabe, M.F.; Evans, J.P.; Van Dijk, A.I.J.M. Trend-preserving blending of passive and active microwave soil moisture retrievals. *Remote Sens. Environ.* **2012**, *123*, 280–297. [CrossRef]
57. Kim, H.; Parinussa, R.; Konings, A.; Wagner, W.; Cosh, M.; Choi, M. Global-scale assessment and combination of SMAP with ASCAT (active) and AMSR2 (passive) soil moisture products. *Remote Sens. Environ.* **2017**. [CrossRef]
58. Rüdiger, C.; Calvet, J.C.; Gruhier, C.; Holmes, T.R.; De Jeu, R.A.M.; Wagner, W. An intercomparison of ERS-Scat and AMSR-E soil moisture observations with model simulations over France. *J. Hydrometeorol.* **2009**, *10*, 431–447. [CrossRef]
59. Entekhabi, D.; Reichle, R.H.; Koster, R.D.; Crow, W.T. Performance metrics for soil moisture retrievals and application requirements. *J. Hydrometeorol.* **2010**, *11*, 832–840. [CrossRef]
60. Taylor, K.E. Summarizing multiple aspects of model performance in a single diagram. *J. Geophys. Res. Atmos.* **2001**, *106*, 7183–7192. [CrossRef]
61. Yee, M.S.; Walker, J.P.; Rüdiger, C.; Parinussa, R.M.; Koike, T.; Kerr, Y. H. A comparison of SMOS and AMSR2 soil moisture using representative sites of the OzNet monitoring network. *Remote Sens. Environ.* **2017**, *195*, 297–312. [CrossRef]